ADVANCED FUNCTIONAL MATERIALS
www.afm-journal.de

Materials Views
www.MaterialsViews.com

Hierarchical Nanowire Arrays Based on ZnO Core–Layered Double Hydroxide Shell for Largely Enhanced Photoelectrochemical Water Splitting

Mingfei Shao, Fanyu Ning, Min Wei, David G. Evans, and Xue Duan**

Well-aligned hierarchical nanoarrays containing ZnO core and layered double hydroxide (LDH) nanoplatelets shell have been synthesized via a facile electrosynthesis method. The resulting ZnO@CoNi–LDH core–shell nanoarray exhibits promising behavior in photoelectrochemical water splitting, giving rise to a largely enhanced photocurrent density as well as stability; much superior to those of ZnO-based photoelectrodes. This is attributed to the successful integration of photogenerated electron–hole separation originating from the ZnO core and the excellent electrocatalytic activity of LDH shell. This work provides a facile and cost-effective strategy for the fabrication of multifunctional nanoarrays with a hierarchical structure, which can be potentially used in energy storage and conversion devices.

1. Introduction

With imminent depletion of global fossil fuels and increasing concern on the climate change, considerable efforts have been devoted to exploiting clean and efficient power sources in the past decade.[1] Photoelectrochemical (PEC) splitting of water into hydrogen and oxygen by the direct use of sunlight is an ideal, renewable method of clean energy production that integrates solar energy collection and water electrolysis into a single photoelectrode. The efficiency and stability of photoanodes are key factors in PEC cells, and a great many semiconductor materials have been used as photoanodes (e.g., ZnO,[2] TiO_2,[3] and α-Fe_2O_3[4]). Although these materials have shown interesting performance, the efficiency of photocatalytic process generally suffers from poor charge transport property and slow interfacial kinetics for water splitting. Recently, considerable interest have been invested to overcome these disadvantages, including tuning compositions (e.g., doping),[5] construction of nanostructured electrodes (e.g., branched nanowire and nanotube array),[6] and loading of cocatalysts (e.g., IrO_2 and Co-based materials).[7] Nevertheless, how to achieve cost-effective photoanodes with high energy conversion efficiency and desirable stability for PEC water splitting remains a challenging goal.

M. F. Shao, F. Y. Ning, Prof. M. Wei, Prof. D. G. Evans, Prof. X. Duan
State Key Laboratory of Chemical Resource Engineering
Beijing University of Chemical Technology
Beijing, 100029, PR China
E-mail: weimin@mail.buct.edu.cn

DOI: 10.1002/adfm.201301889

The integration of promising water oxidation catalyst with a photon-absorbing substrate can provide a substantial reduction in the external power needed to drive water splitting. For example, cobalt–phosphate-based (Co–Pi) materials have been used to improve the photocurrent of PEC electrodes by facilitating electron-hole pair separation and improving O_2 evolution kinetics.[7b,c,d] Layered double hydroxides (LDHs) are layered anionic clays generally expressed by the formula $[M^{II}_{1-x}M^{III}_x(OH)_2]^{z+}(A^{n-})_{z/n}\cdot\gamma H_2O$ (M^{II} and M^{III} are divalent and trivalent metals respectively; A^{n-} is the interlayer anion compensating for the positive charge of the brucite-like layers).[8] The versatility in both chemical composition and structural morphology of LDH materials makes them attractive candidates as electrocatalysts.[9] For the water-splitting application, nanostructured LDHs is particularly relevant on account of their high surface-to-volume ratio and short diffusion length for carrier transport compared with their bulk counterparts. In this regard, the incorporation of semiconductor core–hierarchical LDH shell into a sophisticated nanoarray structure for photoelectrodes would be a preferable resolution in PEC catalysis: (i) the semiconductor core guarantees the utilization of solar energy, giving rise to reduced external power consumption; (ii) the LDH shell as effective co-catalyst increases the reaction kinetics, thus depressing the charge recombination rate; (iii) the hierarchical structure enables a convenient charge transfer to the electrode/electrolyte interface where the oxidation of water molecules occurs.

Herein, we demonstrate the design and fabrication of well-aligned ZnO core@LDH shell hierarchical nanoarrays by direct deposition of LDH nanosheets on ZnO nanowires (NWs) via a facile electrosynthesis method, which exhibit largely enhanced PEC water splitting performance. Various metal oxides@LDH core–shell hierarchical nanoarrays (ZnO@LDH, TiO_2@LDH, and Co_3O_4@LDH) have been prepared with fine control over the shell thickness and morphology; the LDH nanoplatelets were strongly and uniformly anchored onto the surface of semiconductor NWs. The as-obtained ZnO@CoNi-LDH core–shell nanoarray exhibits promising behavior in PEC water splitting, giving rise to a largely enhanced photocurrent density and stability, much superior to those of ZnO-based photoelectrodes. This is attributed to the successful integration of photogenerated electron-hole separation originating from ZnO core and

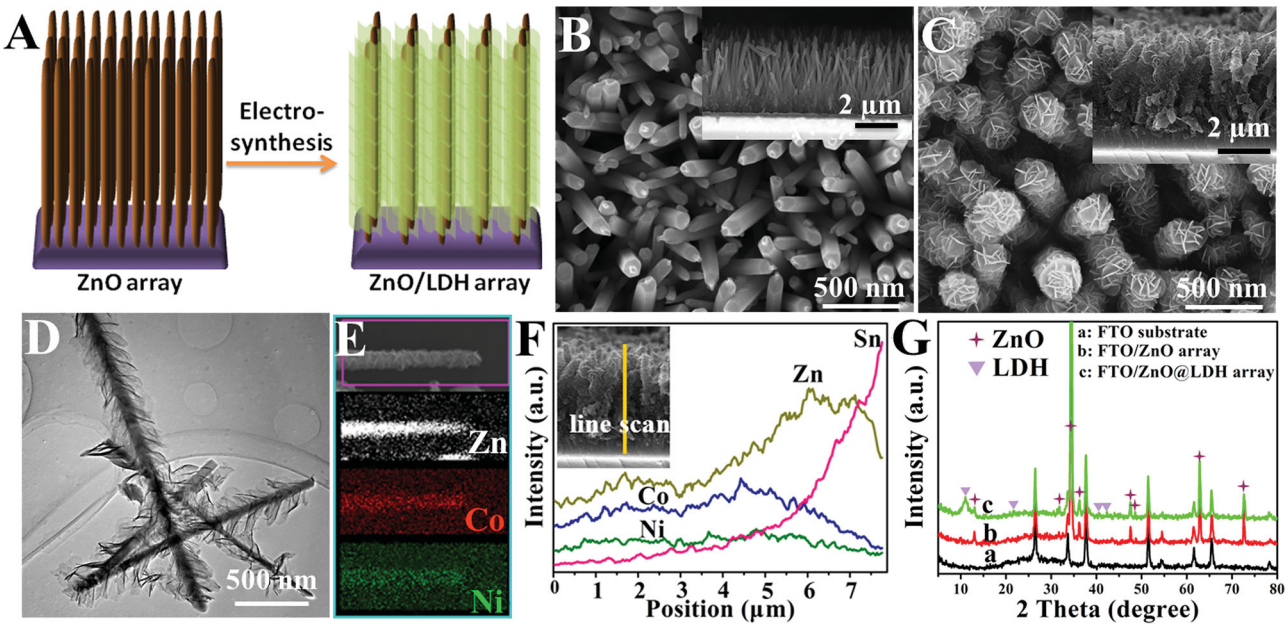

Figure 1. (A) Schematic illustration of the fabrication of ZnO@LDH core–shell NWs array; SEM images of (B) ZnO NWs and (C) ZnO@LDH core–shell NWs array on FTO; (D) TEM image, (E) EDX mapping and (F) line scan results of ZnO@LDH core–shell NWs array; (G) XRD patterns of (a) FTO substrate, (b) ZnO NWs array on FTO, (c) ZnO@CoNi-LDH NWs array on FTO.

excellent electrocatalytic behavior of LDH shell. To the best of our knowledge, this is the first paradigm of sensitizing metal oxides nanowires with inorganic LDH materials for enhanced photoanode property.

2. Results and Discussion

The preparation of ZnO@CoNi-LDH NWs array with core–shell structure on fluorine-doped tin oxide (FTO) substrate is illustrated in **Figure 1**A. The ZnO NWs grown on FTO were prepared *via* a solvothermal method as described previously.[5d] As shown in Figure 1B, the ZnO NWs were vertically aligned to FTO with an average diameter of ~90 nm and a length of ~3.6 μm, respectively. After being coated with LDH nanoflakes (~75 nm in width and ~15 nm in thickness) by an electrosynthesis route, core–shell ZnO@CoNi-LDH nanoarrays with uniformity both in size and morphology were obtained, with intercrossing LDH nanoplatelets perpendicularly grafted to the solid core (Figure 1C and Figure S1, Supporting Information). The core–shell structure was further demonstrated in the TEM image of the resulting ZnO@LDH arrays (Figure 1D), from which the core diameter of ~85 nm and the shell thickness of ~75 nm were identified clearly. EDX mapping analysis (Figure 1E) shows that the zinc is located in the central part of the NWs composite while both cobalt and nickel are homogeneously distributed throughout the whole NWs. The line scanning profile (Figure 1F), combined with the EDX spectrum of ZnO@CoNi-LDH arrays (Figure S2, Supporting Information), further verifies the uniform presence of Zn, Co and Ni (with a Co/Ni molar ratio of ~2.0). Figure 1G shows the XRD patterns of FTO substrate, ZnO/FTO, and ZnO@CoNi-LDH/FTO, respectively. The XRD pattern of ZnO NWs with dominant (002) reflection (Figure 1G, curve b) confirms their preferential anisotropic growth along the [001] direction of FTO. After coating with the LDH layer, the XRD pattern of the resulting material (Figure 1G, curve c) shows a superimposition of a ZnO phase and an LDH phase. The (003), (006), (012) and (107) reflection of a typical LDH material are clearly observed, indicating its high crystallinity. In addition, this method can be readily extended to the fabrication of other semiconductor core–LDH shell arrays. The example of TiO_2@LDH and Co_3O_4@LDH arrays were also synthesized *via* the electrosynthesis method, giving materials with similar core–shell structure and uniform morphology (Figure S3, Supporting Information).

The detailed nanostructure of ZnO@CoNi-LDH is further investigated by high-resolution TEM (HR-TEM). **Figure 2**A shows the LDH nanoflake and ZnO nanowire are densely interconnected, and the HR-TEM image of the nanowire edge section (Figure 2B) provides more compelling evidence on the interface between ZnO nanowire and LDH nanoplatelet. The ZnO core exhibits a distortion of lattice fringes in the interface region (including bending and dislocation), demonstrating a strong interaction between ZnO and LDH.[10] The selected-area electron diffraction (SAED) pattern (Figure 2B, inset) is indicative of the two-component crystalline nature: one set of spots can be indexed to a single crystalline ZnO wurtzite structure along the [100] zone axis; another set of hexagonally arranged spots correspond to the LDH phase. In addition, the HR-TEM image of one LDH nanoflake (Figure S4) and its SAED pattern (Figure S4, inset) confirm the crystal structure of CoNi-LDH, in which the fringes with lattice spacing of 0.24 nm can be indexed to the (012) plane of a CoNi-LDH phase.

X-ray photoelectron spectroscopy (XPS) and extended X-ray absorption fine structure (EXAFS) techniques were employed to give a further insight into the interaction between ZnO core

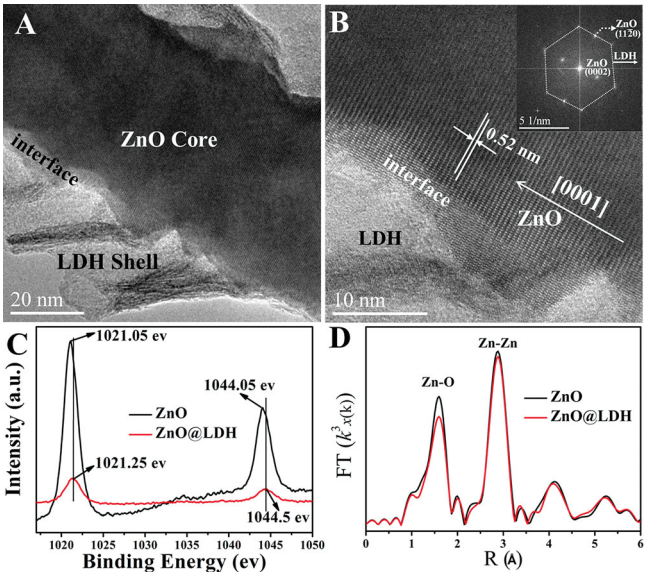

Figure 2. (A) HR-TEM image and (B) magnification of image A for the ZnO@LDH core–shell NWs (inset: the corresponding fast Fourier transform (FFT) pattern); (C) typical Zn 2p XPS spectra and (D) fourier transforms of EXAFS spectra for ZnO NWs and ZnO@LDH core–shell NWs array, respectively.

and LDH shell. Figure 2C shows the typical XPS spectra of ZnO and ZnO@LDH nanoarrays, respectively. For the sample of ZnO NWs, the binding energies of Zn $2p_{1/2}$ and Zn $2p_{3/2}$ are respectively located at 1044.05 and 1021.05 eV, with a spin energy separation of 23 eV, in good agreement with reported data of Zn 2p states in ZnO NWs.[11] After the electrodeposition of LDH shell, both the Zn $2p_{1/2}$ and Zn $2p_{3/2}$ peaks shift to higher energy levels (1044.5 and 1021.25 eV, respectively), along with a sharp decrease in the intensity, suggesting the interaction between ZnO and LDH. The Co 2p and Ni 2p core level spectra of the as-synthesized ZnO@LDH nanoarrays sample were recorded in Figure S5. The Co $2p_{3/2}$ spectrum shows a complex structure broadened by multiplet splitting effects (Figure S5-A). The binding energy of Co $2p_{3/2}$ can be decomposed to 780.1 and 781.6 eV, indicating the presence of Co^{3+} and Co^{2+} oxidation state in the sample with Co^{3+}/Co^{2+} atomic ratio of 0.9 based on the integral peak area. Figure S5-B shows the binding energy of Ni 2p is located at 855.6 eV, corresponding to the Ni(II) oxidation state. Based on the EDS analysis and elemental analysis, the composition of NiCo-LDH shell were determined as $[Ni^{2+}_{0.23}Co^{2+}_{0.24}Co^{3+}_{0.31}(OH)_2]_{0.32}(Cl^-)_{0.32}$.

The fourier transform (FT) magnitudes of the Zn K-edge EXAFS for the ZnO NWs and ZnO@LDH nanoarrays are shown in Figure 2D. For the ZnO NWs sample, the first peak at ~1.6 Å is due to Zn–O coordination in the first shell; the second peak at ~3 Å is attributed to the second Zn–Zn coordination shell.[12] After electrodeposition of LDH layer on ZnO NWs, the Zn–O and Zn–Zn coordination peaks in the FT display a slight decrease, indicating the structural defects induced in the ZnO host lattice by the LDH incorporation. The EXAFS results are consistent with those of HR-TEM and XPS, demonstrating an interaction occurs between ZnO core and LDH shell. This interaction would facilitate the electron transfer at the ZnO/LDH interface and the resulting PEC behavior, which will be discussed in the next section. In addition, no obvious broadening of FT peak was observed for the ZnO@LDH nanoarrays, indicating a low LDH substitution into the ZnO phase.[12a] This is consistent with the result of HR-TEM image (Figure 2B).

Time-dependent experiments were carried out to understand the formation process of such interesting ZnO@LDH core–shell hierarchical array. **Figure 3** shows the scanning electron microscopy (SEM) images of six samples obtained with different electrosynthesis durations. A thin layer of nanoflake-like subunits appears on the surface of ZnO NWs with a short deposition time (30 s, Figure 3A); numerous nanoflakes come into formation on the surface of ZnO NWs with the deposition time of 50 s (Figure 2B). As the reaction time was further prolonged, the LDH nanoflakes with well-defined plate-like morphology grow much bigger and more densely with decreasing interspace. After 300 s of electrodeposition, the whole surface of the electrode is covered with LDH nanoflakes. It is known that light absorption of a material and the migration of the light-induced electrons and holes are the most key factors in controlling a photocatalytic reaction, which is relevant to the electronic structure of the material.[13] The UV-vis absorption spectra of ZnO NWs and ZnO@LDH core–shell nanoarrays with various deposition time show similar absorptive property in the full solar spectrum region (Figure S6), indicating that the introduced LDH shell does not hinder the light absorption of ZnO NWs.

The hierarchical ZnO@LDH core–shell nanoarrays were subsequently investigated as photoanodes in PEC water splitting. As shown in **Figure 4**A, compared with the pristine ZnO NWs, the photocurrent density of ZnO@LDH arrays increases significantly in a potential window from –0.5 to 1.2 V *vs.* Ag/

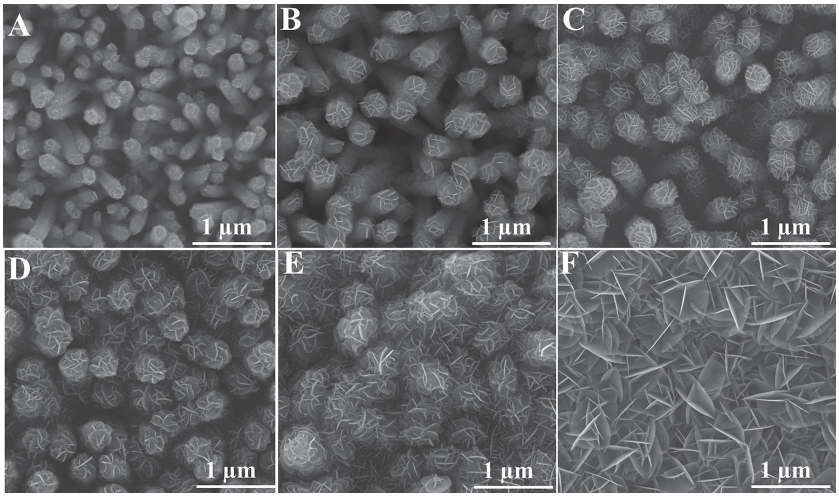

Figure 3. SEM images of ZnO@LDH core–shell nanoarrays obtained with various electrodeposition durations: (A) 30 s, (B) 50 s, (C) 100 s, (D) 150 s, (E) 200 s, (F) 300 s.

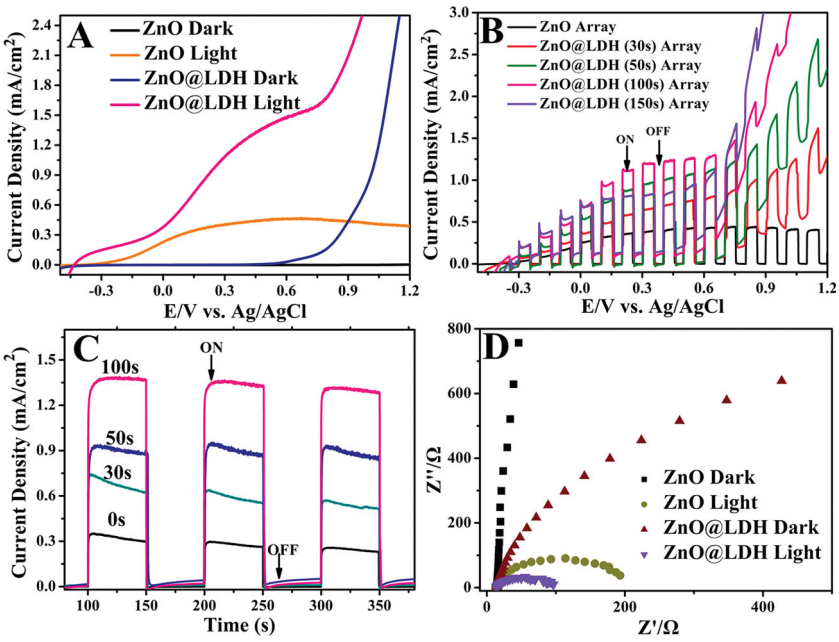

Figure 4. (A) Current-voltage curves of pristine ZnO NWs and ZnO@LDH (100 s) core–shell NWs array in the dark and under illumination at a scan rate of 10 mVs^{-1}; (B) current-voltage behavior of ZnO@LDH core–shell NWs arrays with various LDH deposition time upon chopped light illumination; (C) amperometric *I–t* curves at a potential of 0.5 V for pristine ZnO NWs and ZnO@LDH core–shell NWs arrays with various LDH deposition time; (D) electrochemical impedance spectra (measured at 0.5 V) of pristine ZnO NWs and ZnO@LDH (100 s) core–shell NWs array under illumination.

AgCl. The ZnO@LDH nanoarrays photoanode (with LDH deposition time of 100 s) shows a pronounced photocurrent starting at about –0.3 V, which increases to 1.5 $mAcm^{-2}$ at +0.5 V under illumination. The photocurrent density is about three times larger than that of pristine ZnO NWs at +0.5 V and 7 times at +1.0 V, suggesting the definitely enhanced PEC performance in water splitting by introducing CoNi-LDH shell. The effect of LDH catalysts on water splitting is also evident in the dark scan (Figure S7), in which the onset of electrochemical O_2 evolution shifts to the negative direction (decreasing overpotential) with the increase of LDH deposition time from 0 to 100 s. The results demonstrate that the CoNi-LDH can effectively catalyze water splitting. To further reveal the effect of LDH shell deposited on the ZnO NWs, a series of photocurrent measurements were carried out on ZnO@LDH NWs photoanodes with various LDH deposition time (from 30 to 150 s). The corresponding photocurrent response to light ON–OFF cycling is shown in Figure 4B, from which a steady and prompt photocurrent generation can be observed during on and off cycles of illumination. The photocurrent of ZnO@LDH NWs firstly increases gradually along with the increase of LDH deposition time and reaches a maximum for the ZnO@LDH (100 s) NWs sample. However, the measured photocurrent decreases significantly with further elongation of the deposition time. This result demonstrates that coating of LDH onto ZnO at a suitable level can effectively enhance ZnO photocatalytic activity; while an excess of LDH incorporation leads to a decrease of the photoconversion efficiency, which may result from a dense packing of LDH on the electrode that hinders photon absorption and charge transfer. To examine the photoresponse of the core-shell structure over time, the *I–t* curve of ZnO@LDH NWs at +0.5 V with the deposition time from 0 to 100 s was measured (Figure 4C). Upon illumination at 100 $mWcm^{-2}$, a spike in the photoresponse was observed for all the samples owing to the transient effect in power excitation, and the photocurrent then quickly returned to a steady state. This further confirms that photogenerated electrons promptly transfer from ZnO core to LDH shell. Compared with the reported photocurrent densities for photoelectrodes (usually less than 1 $mAcm^{-2}$ at 0.5 V),[14,5a,6c,7b,d] the results in this work show that the well-aligned ZnO@LDH hierarchical nanowires array photoelectrode exihibits superior PEC performance. It is proposed that the LDH shell and high-quality contact at the ZnO/LDH interface increase the reaction kinetics of water splitting and facilitate the charge transfer to the electrode/electrolyte interface, accounting for the largely enhanced PEC behavior.

Electrochemical impedance spectroscopy (EIS) study provides information about the interfacial property of photoanodes. The semicircle diameter of EIS equals the electron transfer resistance (R_{et}), which controls the electron transfer kinetics of the redox probe at the electrode interface.[15] Figure 4D shows the typical EIS for the ZnO and ZnO@LDH electrode in 0.5 M Na_2SO_4 solution, measured in the dark and illumination (at 100 $mWcm^{-2}$), respectively. The semicircles for both samples are much larger in the dark than with illumination (Figure 4D), demonstrating that the photogenerated charge carriers substantially lower the charge-transfer resistance. In addition, the ZnO@LDH array with smaller diameter was observed both in the dark and under illumination relative to the ZnO NWs, which indicates a conducting effect of the CoNi-LDH shell on the electron-transfer process at the electrode interface. This result is consistent with the photocurrent measurements which show much higher photocurrent density for the ZnO@LDH array. Furthermore, the R_{et} decreases significantly as the LDH deposition time increases from 0 to 100 s (Figure S8); while it turns to increase with a further enhancement of deposition time from 100 to 150 s, in accordance with the results of current-voltage behavior of ZnO@LDH core–shell NWs arrays (Figure 4B).

To further evaluate the enhanced PEC water oxidation performance of the ZnO@LDH electrode, incident-photon-to-current-conversion efficiency (IPCE) was measured for the core-shell nanowire arrays with LDH deposition time from 0 to 150 s (**Figure 5**A). It was found that the UV–vis transmittance spectra for pristine ZnO NWs and ZnO@LDH core-shell NWs are almost identical, suggesting that the LDH co-catalyst does not affect the light absorption ability of the materials (Figure S6). IPCE is expressed as IPCE = $(1240I)/(\lambda P_{light})$, where I is the photocurrent density (mA/cm^2); λ is the incident light wavelength (nm), and P_{light} (mW/cm^2) is the power

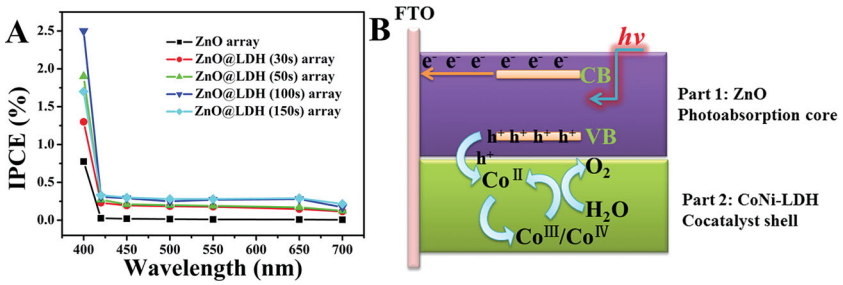

Figure 5. (A) IPCEs for ZnO@LDH electrode with various LDH deposition time, measured in the wavelength range 400–700 nm at applied voltage of +0.50 V. (B) Schematic illustration of the photoelectrochemical water oxidation process by the as-obtained ZnO@LDH core–shell NWs array.

density of monochromatic light at a specific wavelength. In comparison with the pristine ZnO NWs, the ZnO@LDH core-shell nanowire arrays show substantially enhanced IPCE. For instance, the IPCE of the pristine ZnO NWs, ZnO@LDH (30 s), ZnO@LDH (50 s) and ZnO@LDH (100 s) at the incident wavelength of 400 nm are 0.78, 1.3, 1.9, and 2.5%, respectively; while a decrease was observed in the sample of ZnO@LDH (150 s): 1.7%. As demonstrated in Figure 4B, by using a water oxidation cocatalyst, the PEC performance of ZnO@LDH can be largely enhanced, resulting in more than 7 times (at +1.0 V) higher full-spectrum photocurrent compared with unmodified ZnO NWs.

Recently, the photoelectrochemical water oxidation by cobalt/metal oxide systems has been reported, which usually involves the redox couples (Co^{II}/Co^{III} and Co^{III}/Co^{IV}) in a cycling process.[7c,d,16] In this work, photogenerated holes in ZnO core are transferred to the core-shell interface to oxidize Co^{II} to Co^{III}/Co^{IV} species in CoNi-LDH shell, which serves as co-catalysts to promote the water splitting reaction (Figure 5B). The high-quality contact at the ZnO/LDH interface allows fast and efficient transfer of the photogenerated holes from the ZnO core to the LDH shell, which depresses anodic decomposition/corrosion and improves the photodevice stability. Moreover, the LDH as effective co-catalyst accelerates the reaction kinetics of water splitting, and therefore reduces the charge recombination rate. In addition, the chemical stability is an important requirement for photoanodes in PEC water splitting for a long-term application. Figure S9 shows that the photocurrent response was almost identical over 30 cycles, indicating a good stability of this structure. Therefore, the construction of ZnO@LDH core-shell NWs demonstrates an efficient way to couple an oxygen evolution catalyst with a photoanode for sustainable and affordable solar fuel technologies.

3. Conclusions

The well-aligned hierarchical heterostructure arrays with ZnO NW core and LDH nanoplatelets shell have been successfully fabricated *via* a facile and effective electrosynthesis strategy. The resulting core–shell ZnO@LDH NW array exhibits significantly enhanced efficient in PEC water-splitting, including large photocurrent and high stability, much superior to pristine ZnO NWs and most of photoanodes reported previously. This can be ascribed to the specific hierarchical core–shell structure and high electrocatalytic activity, which improves the photogenerated charges separation and accelerates the kinetics of water splitting. In addition, this method can be extended to the preparation of TiO_2@LDH and Co_3O_4@LDH core–shell arrays with prospective physiochemical property. Therefore, this work demonstrates the fabrication of metal oxides NW core–functionalized LDH shell hierarchical structures, which have potential applications in a variety of fields including energy storage and conversion, photoelectric devices and sensors.

4. Experimental Section

Preparation of ZnO@CoNi-LDH Core–Shell NWs Arrays: First, self-supported ZnO NWs were prepared by a facile hydrothermal synthesis method according to previous report.[17] Briefly, 100 mL of a 0.06 M solution of zinc acetate in absolute ethanol was prepared with ultrasonic agitation. A thin layer of ZnO seeds were obtained by spin-coating of the above solution on the pre-treated FTO substrates, followed by annealing at 350 °C for 30 min. The seeded substrates were suspended horizontally in a reagent solution containing 0.06 M zinc nitrate and 0.06 M HMT in a Teflon vessel, and then sealed in an autoclave and heated to 110 °C for 24 h for nanowire growth. The nanowire substrate was removed from the autoclave, washed thoroughly with distilled water and dried in air. Subsequently, the obtained ZnO nanowire substrate was used as the working electrode and placed in an electrochemical cell which was assembled in a three-electrode configuration, by using platinum as the counter electrode and Ag/AgCl as the reference electrode. The electrolyte for electrodeposition of CoNi-LDH was obtained by dissolving $CoCl_2{\cdot}6H_2O$ (1.784 g) and $Ni(NO_3)_2{\cdot}6H_2O$ (2.181 g) in 50 mL of distilled water. The potentiostatic deposition was carried out at a potential of –1.0 V vs. Ag/AgCl. The resulting ZnO@LDH NWs array was withdrawn and rinsed with distilled water.

Preparation of Co_3O_4 NWs Arrays: The Co_3O_4 NWs array was fabricated by a simple hydrothermal method.[18] Typically, 5 mmol of $Co(NO_3)_2{\cdot}6H_2O$, 10 mmol of NH_4F, and 25 mmol of $CO(NH_2)_2$ were dissolved in 50 mL of water under stirring. The homogeneous solution was then transferred into a Teflon-lined stainless steel autoclave. Subsequently, a piece of clean FTO substrate was immersed into the reaction solution. The autoclave was sealed and maintained at 120 °C for 5 h. After the reaction, the substrate was withdrawn and rinsed with distilled water several times in order to remove the free nanoparticle debris and residual reactant. Finally, the substrate was calcinated at 400 °C in air for 4 h.

Preparation of TiO_2 NWs Arrays: The TiO_2 nanorods array was prepared using a hydrothermal synthesis reported previously.[19] Briefly, 12 mL of deionized water was mixed with 12 mL of concentrated hydrochloric acid (mass fraction 36.5–38%). The mixture was stirred at ambient temperature for 5 min followed by addition of 0.4 mL of titanium butoxide. After it was stirred for another 5 min, the mixture was placed in a Teflon-lined stainless steel autoclave. One piece of FTO substrate was then placed at an angle against the inner wall of reactor with the conductive side facing down. The hydrothermal synthesis was performed at 150 °C for 20 h; finally the FTO substrate was rinsed extensively with deionized water, and dried in ambient air.

Preparation of Co_3O_4@LDH and TiO_2@LDH Core–Shell NWs Arrays: The obtained Co_3O_4 or TiO_2 nanowire substrate was used as the working electrode and placed in an electrochemical cell which was assembled in a three-electrode configuration, by using platinum as

the counter electrode and Ag/AgCl as the reference electrode. The electrolyte for electrodeposition of CoNi-LDH shell was obtained by dissolving $CoCl_2{\cdot}6H_2O$ (1.784 g) and $Ni(NO_3)_2{\cdot}6H_2O$ (2.181 g) in 50 mL of distilled water. The potentiostatic deposition was carried out at a potential of –1.0 V vs. Ag/AgCl. The resulting Co_3O_4@LDH and TiO_2@LDH NWs arrays were withdrawn and rinsed thoroughly with distilled water.

Sample Characterization: Powder X-ray diffraction patterns of the core–shell microsphere samples were collected on a Shimadzu XRD-6000 diffractometer using a Cu Kα source, with a scan step of 0.02° and a scan range between 3° and 80°. X-ray photoelectron spectra (XPS) were recorded on a Thermo VG ESCALAB 250 X-ray photoelectron spectrometer at a pressure of about 2×10^{-9} Pa using Al Kα X-rays as the excitation source. The morphology of the microspheres was investigated using a scanning electron microscope (SEM; Zeiss SUPRA 55) with an accelerating voltage of 20 kV, combined with energy dispersive X-ray spectroscopy (EDX) for the determination of metal composition. Transmission electron microscopy (TEM) images were recorded with Philips Tecnai 20 and JEOL JEM-2010 high-resolution transmission electron microscopes. The accelerating voltage was 200 kV in each case. Solid-state UV–vis diffuse reflectance spectra were recorded at room temperature in air by means of a Shimadzu UV-3000 spectrometer equipped with an integrating sphere attachment using $BaSO_4$ as background.

Photoelectrochemical Experiments: All PEC studies were operated on an electrochemical workstation (CHI 660C, CH Instruments Inc., Shanghai) in a home-built three-electrode optical cell using Ag/AgCl as the reference electrode and a Pt wire as the counter electrode. Measurements were performed in a 0.5 M Na_2SO_4 (pH 6.8) solution as supporting electrolyte medium. The pristine ZnO NWs and ZnO@LDH NWs were fabricated respectively as photoanode with an area of ~2 cm^2. The watersplitting photoelectrode was illuminated at 100 $mWcm^{-2}$ from a 150 W xenon lamp. Amperometric *I–t* curves of ZnO@LDH NWs arrays were recorded at an applied voltage of +0.5 V at 100 $mWcm^{-2}$. The sample was illuminated from the back side of the photoanode at room temperature.

Supporting Information

Supporting Information is available from the Wiley Online Library or from the author.

Acknowledgements

This work was supported by the 973 Program (Grant No. 2011CBA00504), the National Natural Science Foundation of China (NSFC) and Beijing Natural Science Foundation (2132043). M. Wei particularly appreciates the financial aid from the China National Funds for Distinguished Young Scientists of the NSFC.

Received: June 13, 2013
Revised: July 9, 2013
Published online: August 23, 2013

[1] a) B. C. H. Steele, A. Heinzel, *Nature* **2001**, *414*, 345; b) M. Lefèvre, E. Proietti, F. Jaouen, J.-P. Dodelet, *Science* **2009**, *324*, 71; c) M. Grätzel, *Nature* **2001**, *414*, 338; d) D. M. Guldi, G. M. A. Rahman, M. Prato, N. Jux, S. Qin, W. Ford, *Angew. Chem. Int. Ed.* **2005**, *44*, 2015; e) H. Li, Z. Wang, L. Chen, X. Huang, *Adv. Mater.* **2009**, *45*, 4593; f) M. Q. Zhao, Q. Zhang, J. Q. Huang, F. Wei, *Adv. Funct. Mater.* **2012**, *22*, 675; g) L. J. Murray, M. Dincă, J. R. Long, *Chem. Soc. Rev.* **2009**, *38*, 1294; h) X. Chen, L. Liu, P. Y. Yu, S. S. Mao, *Science* **2011**, *331*, 746; i) J. L. Gunjakar, I. Y. Kim, J. M. Lee, N. S. Lee, S. J. Hwang, *Energy Environ. Sci.* **2013**, *6*, 1008.

[2] a) A. Wolcott, W. A. Smith, T. R. Kuykendall, Y. Zhao, J. Z. Zhang, *Adv. Funct. Mater.* **2009**, *19*, 1849; b)Y. K. Hsu, Y. G. Lin, Y. C. Chen, *Electrochem. Commun.* **2011**, *13*, 1383.

[3] a) A. J. Cowan, J. Tang, W. Leng, J. R. Durrant, D. R. Klug, *J. Phys. Chem. C* **2010**, *114*, 4208; b) P. Hartmann, D. K. Lee, B. M. Smarsly, J. Janek, *ACS Nano* **2010**, *4*, 3147; c) J. H. Bang, P. V. Kamat, *Adv. Funct. Mater.* **2010**, *20*, 1970; d) Y. Hou, X. Y. Li, Q. D. Zhao, X. Quan, G. H. Chen, *Adv. Funct. Mater.* **2010**, *20*, 2165.

[4] a) N. T. Hahn, H. Ye, D. W. Flaherty, A. J. Bard, C. B. Mullins, *ACS Nano* **2010**, *4*, 1977; b) L. Li, Y. Yu, F. Meng, Y. Tan, R. J. Hamers, S. Jin, *Nano Lett.* **2012**, *12*, 724; c) S. D. Tilley, M. Cornuz, K. Sivula, M. Grätzel, *Angew. Chem. Int. Ed.* **2010**, *122*, 6549.

[5] a) S. Hoang, S. Guo, N. T. Hahn, A. J. Bard, C. B. Mullins, *Nano Lett.* **2012**, *12*, 26; b) M. Xu, P. Da, H. Wu, D. Zhao, G. Zheng, *Nano Lett.* **2012**, *12*, 1503; c) I. Cesar, A. Kay, J. A. G. Martinez, M. Grätzel, *J. Am. Chem. Soc.* **2006**, *128*, 4582; d) H. M. Chen, C. K. Chen, Y. Chang, C. Tsai, R. Liu, S. Hu, W. Chang, K. H. Chen, *Angew. Chem. Int. Ed.* **2010**, *49*, 5966; e) Y. Myung, D. M. Jang, T. K. Sung, Y. J. Sohn, G. B. Jung, Y. J. Cho, H. S. Kim, J. Park, *ACS Nano* **2010**, *4*, 3789.

[6] a) Z. Yin, Z. Wang, Y. Du, X. Qi, Y. Huang, C. Xue, H. Zhang, *Adv. Mater.* **2012**, *24*, 5374; b) Y. Qiu, K. Yan, H. Deng, S. Yang, *Nano Lett.* **2012**, *12*, 407; c) N. K. Allam, A. J. Poncheri, M. A. El-Sayed, *ACS Nano* **2011**, *5*, 5056; d) M. J. Bierman, S. Jin, *Energy Environ. Sci.* **2009**, *2*, 1050.

[7] a) S. D. Tilley, M. Cornuz, K. Sivula, M. Grätzel, *Angew. Chem. Int. Ed.* **2010**, *49*, 6405; b) D. K. Zhong, D. R. Gamelin, *J. Am. Chem. Soc.* **2010**, *132*, 4202; c) M. Barroso, A. J. Cowan, S. R. Pendlebury, M. Grätzel, D. R. Klug, J. R. Durrant, *J. Am. Chem. Soc.* **2011**, *133*, 14868; d) K. J. McDonald, K. Choi, *Chem. Mater.* **2011**, *23*, 1686; e) E. M. P. Steinmiller, K. S. Choi, *PNAS* **2009**, *106*, 20633; f) V. Artero, M. Chavarot-Kerlidou, M. Fontecave, *Angew. Chem. Int. Ed.* **2011**, *50*, 7238; g) Y. Hou, F. Zuo, A. Dagg, P. Feng, *Angew. Chem. Int. Ed.* **2013**, *125*, 1286.

[8] a) A. M. Fogg, V. M. Green, H. G. Harvey, D. O'Hare, *Adv. Mater.* **1999**, *11*, 1466; b) Z. Gu, A. C. Thomas, Z. P. Xu, J. H. Campbell, G. Q. Lu, *Chem. Mater.* **2008**, *20*, 3715; c) U. Costantino, N. Coletti, M. Nocchetti, *Langmuir* **1999**, *15*, 4454; d) Q. Wang, D. O'Hare, *Chem. Rev.* **2012**, *112*, 4124; e) M. Shao, F. Ning, J. Zhao, M. Wei, D. G. Evans, X. Duan, *J. Am. Chem. Soc.* **2012**, *134*, 1071; f) J. L. Gunjakar, T. W. Kim, H. N. Kim, I. Y. Kim, S. J. Hwang, *J. Am. Chem. Soc.* **2011**, *133*, 14998.

[9] a) D. Shan, S. Cosnier, C. Mousty, *Anal. Chem.* **2003**, *75*, 3872; b) D. Shan, W. Yao, H. Xue, *Biosens. Bioelectron.* **2007**, *23*, 432; c) M. Shao, J. Han, W. Shi, M. Wei, X. Duan, *Electrochem. Commun.* **2010**, *12*, 1077; d) J. Liu, Y. Li, X. Huang, G. Li, Z. Li, *Adv. Funct. Mater.* **2008**, *18*, 1448.

[10] a) F. R. Fan, Y. Ding, D. Y. Liu, Z. Q. Tian, Z. L. Wang, *J. Am. Chem. Soc.* **2009**, *131*, 12036; b) S. Bernal, R. T. Baker, A. Burrows, J. J. Calvino, C. J. Kiely, C. Lopez-Cartes, J. A. Perez-Omil1, J. M. Rodriguez-Izquierdo, *Surf. Interface Anal.* **2000**, *29*, 411.

[11] J. Liu, X. Li, L. Dai, *Adv. Mater.* **2006**, *18*, 1740.

[12] a) T. Liu, H. Xu, W. S. Chin, Z. Yong, A. T. S. Wee, *J. Phys. Chem. C* **2008**, *112*, 3489; b) J. Segura-Ruiz, G. Martínez-Criado, M. H. Chu, S. Geburt, C. Ronning, *Nano Lett.* **2011**, *11*, 5322.

[13] a) X. Chen, J. Ye, S. Ouyang, T. Kako, Z. Li, Z. Zou, *ACS Nano* **2011**, *5*, 4310; b) B. Klahr, S. Gimenez, F. Fabregat-Santiago, T. Hamann, J. Bisquert, *J. Am. Chem. Soc.* **2012**, *134*, 4294.

[14] a) X. Yang, A. Wolcott, G. Wang, A. Sobo, R. C. Fitzmorris, F. Qian, J. Z. Zhang, Y. Li, *Nano Lett.* **2009**, *9*, 2331; b) A. Wolcott, W. A. Smith, T. R. Kuykendall, Y. Zhao, J. Z. Zhang, *Small* **2009**, *5*,

104; c) D. Qin, C. Tao, S. A. Friesen, T. Wang, O. K. Varghese, N. Bao, Z. Yang, T. E. Mallouk, C. A. Grimes, *Chem. Commun.* **2012**, *48*, 729.

[15] a) J. F. Zang, S. J. Bao, C. M. Li, H. J. Bian, X. Q. Cui, Q. L. Bao, C. Q. Sun, J. Guo, K. R. Lian, *J. Phys. Chem. C* **2008**, *112*, 14843; b) A. D. Fabio, A. Giorgi, M. Mastragostino, F. Soavi, *J. Electrochem. Soc.* **2001**, *148*, A845.

[16] a) E. M. P. Steinmiller, K. S. Choi, *PNAS* **2009**, *106*, 20633; b) C. L. Farrow, D. K. Bediako,Y. Surendranath, D. G. Nocera, S. J. L. Billinge, *J. Am. Chem. Soc.* **2013**, *135*, 6403; c) M. Liao, J. Feng, W. Lou, Z. Wang, J. Zhang, Z. Li, T. Yu, Z. Zou, *Adv. Funct. Mater.* **2012**, *22*, 3066.

[17] H. M. Chen, C. K. Chen, Y. Chang, C. Tsai, R. Liu, S. Hu, W. Chang, K. H. Chen, *Angew. Chem. Int. Ed.* **2010**, *49*, 5966.

[18] J. Jiang, J. P. Liu, X. T. Huang, Y. Y. Li, R. M. Ding, X. X. Ji, Y. Y. Hu, Q. B. Chi, Z. H. Zhu, *Cryst. Growth Des.* **2010**, *10*, 70.

[19] H. Wang, Y. Bai, H. Zhang, Z. Zhang, J. Li, L. Guo, *J. Phys. Chem. C* **2010**, *114*, 16451.